# The fiber knob protein of human adenovirus type 49 mediates highly efficient and promiscuous infection of cancer cell lines using a novel cell entry mechanism

Alexander T. Baker[1,2], Gareth Marlow[1], James A. Davies[1], Elise Moses[1], Rosie M. Mundy[1], David K. Cole[3], Pierre J. Rizkallah[3], Alan L. Parker[1*]

[1]Division of Cancer and Genetics, School of Medicine, Cardiff University, Heath Park, Cardiff, CF14 4XN, UK.
[2]Current address: Department of Haematology and Oncology, Mayo Clinic, 13208 E Shea Blvd, Scottsdale, Arizona, 85259, USA
[3]Division of Infection and Immunity, School of Medicine, Cardiff University, Heath Park, Cardiff, CF14 4XN, UK.
*Corresponding Author, ParkerAL@Cardiff.ac.uk

**Correspondence:**
Dr Alan Parker
Division of Cancer and Genetics
Cardiff University
Heath Park
Cardiff
CF14 4XN
Telephone: +44 2922 510 231
Email: ParkerAL@cardiff.ac.uk

**Word count**
Abstract: 249
Importance: 150
Main text: 4972
Figure legends: 929
Figure count: 5 Figures plus 2 tables

Running title: Ad49 fiber knob permits promiscuous cell entry

# Abstract

The human adenovirus (HAdV) phylogenetic tree is diverse, divided across seven species and comprising over 100 individual types. Species D HAdV are rarely isolated with low rates of pre-existing immunity, making them appealing for therapeutic applications. Several species D vectors have been developed as vaccines against infectious diseases where they induce robust immunity in pre-clinical models and early phase clinical trials. However, many aspects of the basic virology of species D HAdV, including their basic receptor usage and means of cell entry, remain understudied.

Here, we investigated HAdV-D49, which previously has been studied for vaccine and vascular gene transfer applications. We generated a pseudotyped HAdV-C5 presenting the HAdV-D49 fiber knob protein (HAdV-C5/D49K). This pseudotyped vector was efficient at infecting cells devoid of all known HAdV receptors, indicating HAdV-D49 uses an unidentified cellular receptor. Conversely, a pseudotyped vector presenting the fiber knob protein of the closely related HAdV-D30 (HAdV-C5/D30K), differing in four amino acids to HAdV-D49, failed to demonstrate the same tropism. These four amino acid changes resulted in a change in isoelectric point of the knob protein, with HAdV-D49K possessing a basic apical region compared to a more acidic region in HAdV-D30K. Structurally and biologically we demonstrate that HAdV-D49 knob protein is unable to engage CD46, whilst potential interaction with CAR is extremely limited by extension of the DG loop. HAdV-C5/49K efficiently transduced cancer cell lines of pancreatic, breast, lung, oesophageal and ovarian origin, indicating it may have potential for oncolytic virotherapy applications, especially for difficult to transduce tumour types.

54 ## Importance

55 Adenoviruses are powerful tools experimentally and clinically. To maximise efficacy, the development of
56 serotypes with low pre-existing levels of immunity in the population is desirable. Consequently,
57 attention has focussed on those derived from species D, which have proven robust vaccine platforms.
58 This widespread usage is despite limited knowledge in their basic biology and cellular tropism.

59 We investigated the tropism of HAdV-D49, demonstrating it uses a novel cell entry mechanism that
60 bypasses all known HAdV receptors. We demonstrate, biologically, that a pseudotyped HAdV-C5/D49K
61 vector efficiently transduces a wide range of cell lines, including those presenting no known adenovirus
62 receptor. Structural investigation suggests that this broad tropism is the result of a highly basic
63 electrostatic surface potential, since a homologous pseudotyped vector with a more acidic surface
64 potential, HAdV-C5/D30K, does not display a similar pan-tropism. Therefore, HAdV-C5/D49K may form a
65 powerful vector for therapeutic applications capable of infecting difficult to transduce cells.

66 # Introduction:

67 Human adenoviruses are divided into seven species, A-G(1). These non-enveloped, icosahedral viruses
68 have garnered significant interest as therapeutic vectors since they can be grown and purified to high
69 titers, and because the double-stranded DNA genome is readily amenable to genetic modification,
70 enabling the overexpression of therapeutic transgenes(2, 3). Similar techniques can also be applied to
71 genetically alter the virus structural genes, creating modified viral tropisms which are retained by
72 progeny virions after replication.

73 Clinically, adenoviruses have been developed as vectors for gene therapy, vaccines, and as oncolytic
74 virotherapies(1, 4, 5). However, efficacy in these applications can be hampered by pre-existing immunity
75 against the therapeutic vector in the population resulting from prior exposure to the wild type
76 pathogen. Such pre-existing immunity is likely to reduce the therapeutic index of such systems, due to
77 rapid and efficient removal of the engineered therapeutic agent by the reticuloendothelial system(6, 7).
78 This is especially relevant where the therapeutic is based on the most commonly studied species C
79 adenovirus, human adenovirus type 5 (HAdV-C5), where neutralising antibodies are found in ~90% of
80 patients from sub-Saharan Africa and ~30% of a Scottish patient cohort(8, 9).

81 A promising means to circumvent pre-existing immunity is through the development of viruses with
82 naturally low seroprevalence rates as therapeutic agents. For example, vaccines have been developed
83 using chimpanzee adenoviruses which have little to no seroprevalence in humans. However, it appears a
84 significant percentage of some populations may still harbour some immunity to chimpanzee
85 adenoviruses, as observed in a cohort from China(10).

86 Most attempts to develop adenoviruses with low seroprevalence have focused on those derived from
87 species B or D, due to their comparative rarity(5, 9, 11). The most clinically advanced of these are HAdV-
88 D26 and Enadenotucirev (formerly ColoAd1)(12). Enadenotucirev was developed by evolution of a panel

89 of different adenovirus strains to select for recombinants with rapid replication in tumour cells. The
90 resultant recombinant was predominantly HAdV-B11 with some elements of HAdV-B3, and has
91 progressed into clinical trials as a novel cancer therapeutic(13, 14). HAdV-D26, is a replication deficient
92 vector and the basis of the Ad26.ZEBOV vaccine against Ebola virus, currently under evaluation in the
93 PREVAIL and PREVAC studies(15, 16).

94 Many species D adenoviruses have previously been evaluated for their potential as vaccines, gene
95 therapies, and oncolytic viruses(1, 5, 9, 11). One with particularly low seroprevalence rates is HAdV-D49.
96 In a cohort of 100 Belgian individuals only 2% had HAdV-D49 positive sera, whilst no pre-existing
97 immunity against HAdV-D49 was detected in 103 Scottish patients(8, 17). Prevalence is somewhat
98 higher in sub-saharan Africa with 22% of 200 patients presenting neutralising antibodies (nAbs),
99 highlighting significant geographical variation in seroprevalence(9).

100 HAdV-D49 was first isolated from the faeces of a human with no observed disease, and later from Dutch
101 patients(18, 19). It was then isolated from nosocomial epidemic keratoconjunctivitis infections(20, 21),
102 but is most associated with patients who are immunocompromised due to HIV infection(22). A study of
103 adenovirus infections in patients from the UK and Netherlands found 11 instances of HAdV-D49
104 infection in 183 HIV positive patients (6% HAdV-D49 positive), compared to just two instances in 2301
105 tested healthy patients (0.09% HAdV-D49 positive)(19).

106 Previous studies suggest that HAdV-D49 may be effective as a vaccine vector. A vaccine vector based on
107 HAdV-D49 has been evaluated previously for its ability to protect against simian immunodeficiency virus
108 (SIV) challenge. This vector induced strong anti-SIVGag $CD8^+$ mediated immunity to SIV, greater than the
109 comparable HAdV-C5 based vector(23). Another study sought to exploit HAdV-D49 a gene therapy to
110 reduce excessive smooth muscle cell proliferation in vascular conduits following bypass grafting. This
111 study demonstrated that HAdV-D49 was efficient at infecting endothelial cells and vascular smooth

112 muscle cells, even after short exposure times(8). Studies in CAR, CD46, and α2-3 linked sialic acid
113 expressing cells have previously suggested that HAdV-D49 may engage CD46 as a cellular receptor,
114 although the effects observed were small(23).

115 Despite these studies and the development of HAdV-D49 as a therapeutic agent, there remains little
116 information surrounding the basic biology of HAdV-D49 and its means of cellular engagement. Here, we
117 investigate the tropism of HAdV-D49, focussing on the fiber knob protein as the major mediator of
118 cellular attachment, and evaluate the potential utility of a pseudotyped HAdV-C5/D49K vector to infect
119 a range of cancer cell lines.

120 # Results and Discussion

121 ## HAdV-C5/D49K is not dependent on any known adenovirus receptor for cell entry

122 To investigate the receptor usage of human adenovirus type 49 fiber knob protein we generated a
123 replication incompetent HAdV-C5 vector pseudotyped with the fiber knob protein of HAdV-D49 (HAdV-
124 C5/D49K), expressing either green fluorescent protein (GFP) or luciferase as transgenes. We also
125 produced a replication deficient HAdV-C5 based pseudotyped vector with the whole fiber protein,
126 including both the fiber shaft and fiber knob of HAdV-D49, expressing luciferase (HAdV-C5/D49F). This
127 pseudotyping approach is a well-established means to investigate the fiber knob in the context of a well
128 understood, replication incompetent virus(1, 24). Using these pseudotyped vectors, we performed
129 transduction assays in CHO cells expressing common adenovirus receptors (Figure 1). CHO-K1 cells do
130 not express any known adenovirus receptor, whilst CHO-CAR cells express the HAdV-C5 receptor,
131 coxsackie and adenovirus receptor (CAR), and CHO-BC1 cells express the BC1 isoform of CD46, the major
132 receptor for species BI adenovirus, which includes HAdV-B35.

133 The ability of HAdV-C5/D49K to transduce cell lines was compared to similar GFP expressing replication
134 incompetent vectors HAdV-C5 and HAdV-C5/B35K, which engage CAR and CD46 as receptors,
135 respectively(24–26). HAdV-C5/D35K was unable to transduce CHO-CAR, due to the lack of CD46, whilst
136 HAdV-C5 transduced CHO-CAR cells efficiently due to the high levels of CAR expressed. HAdV-C5/D49K
137 transduced CHO-CAR cells efficiently, but slightly less so (by ~20%) compared to HAdV-C5 (Figure 1A). In
138 CHO-BC1 cells, transduction by HAdV-C5 was inefficient, due to the absence of CAR, whilst HAdV-C5/B35
139 transduced these cells with almost 100% efficiency, due to the presence of high affinity HAdV-B35
140 receptor, CD46. HAdV-C5/D49K demonstrated a similar ability to HAdV-C5-B35K to transduce CHO-BC1
141 cells (Figure 1B). In CHO-K1 cells neither HAdV-C5 nor HAdV-C5/B35K were able to efficiently transduce
142 the cells due to the absence of known adenovirus cell surface receptors. HAdV-C5/D49K, however, was

143 able to transduce these cells efficiently, indicating that HAdV-D49K is able to infect cells efficiently and
144 independently of CAR or CD46 (Figure 1C), thus indicating HAdVC5/D49K engages an alternative cellular
145 receptor. Interestingly, we also observed, in this and later experiments, that HAdV-C5/D49K was less
146 efficient at infecting CHO-CAR cells (Figure 1A) compared to non-CAR expressing CHO cell types (Figure
147 1B-C). These data indicate that the presence of CAR may actively reduce the efficiency of transduction of
148 HAdVC5/D49K compared to levels of transduction in the absence of CAR in the same cell line
149 background.

150 At 385 amino acids in length, the native HAdV-D49 protein is significantly shorter than the equivalent
151 HAdV-C5 fiber protein, which is 581 amino acids in length. This manifests as a naturally shorter and less
152 flexible fiber shaft in HAdV-D49 compared to that of HAdV-C5. This shortened fiber shaft length can
153 impact upon viral infectivity, resulting in trapping of adenoviral particles within late endosomes due to
154 the decreased endosomolytic activity of shorter shafted adenoviral particles(27). To assess the impact of
155 pseudotyping the entire short fiber protein from HAdV-D49 on viral infectivity, we performed similar
156 transduction assays using CHO-K1 cells. Consistent with engaging an alternative receptor on CHO-K1
157 cells, the HAdV-C5/D49F whole-fiber pseudotyped vector efficiently transduced CHO-K1 cells, where
158 HAdV-C5 was unable. Also consistent with shorter shafted HAdVs displaying reduced infectivity due to
159 less efficient intracellular trafficking post-entry, the HAdV-C5/D49F was less efficient than the "knob-
160 only" pseudotype HAdV-C5/D49K at infecting CHO-K1 cells (Figure 1D).

161 We performed similar transduction assays using CHO-K1 and SKOV-3 ovarian cancer cells with and
162 without pre-treatment with either heparinase or neuraminidase to determine the ability of
163 HAdVC5/D49K to bind heparan sulphate proteoglycans (HSPGs) or sialic acid, respectively, to mediate
164 cellular infection (Figure 2). As a positive control for heparinase activity we compared HAdV-C5/D49K
165 infectivity to that of HAdV-C5 in the presence and absence of coagulation factor X (FX), a blood
166 coagulation factor which can facilitate infection of some adenovirus by binding to the viral hexon and

167 cellular heparan sulfate proteoglycans (HSPGs)(28). We observed in CHO-K1 and SKOV-3 cells that
168 transduction levels of HAdV-C5 alone were poor (Figure 2A, B), but were significantly enhanced by the
169 presence of FX, enabling cell entry through cellular HSPGs (29–31). Treatment with heparinase to cleave
170 HSPGs reduced transduction efficiency to that of HAdV-C5 alone. HAdV-C5/D49K transduction efficiency
171 was unaffected by treatment with heparinase (Figure 2A, B), indicating that HAdV-D49 is unlikely to
172 utilise HSPGs for cell entry.

173 Treatment with neuraminidase to remove cellular sialic acid did not alter the ability of any of the viruses
174 to transduce CHO-K1 cells (Figure 2C), as we previously demonstrated to show the involvement of sialic
175 acid in HAdV-C5/D26K infection(24). In SKOV-3 cells, removal of sialic acid actually enhanced the
176 transduction mediated by HAdV-C5/D49K and HAdV-C5/B35K, an effect which we have previously
177 observed by neuraminidase treatment in SKOV-3 cells (Figure 2D)(24, 32, 33). This effect could be a
178 result of the removal of sialic acid enhancing non-specific charge-based interactions between the cell
179 surface and viral capsid. Regardless, these data do not support a role for sialic acid in HAdV-C5/D49K cell
180 infection.

181 The transduction affinity of HAdV-C5/D49K in the experiments in Figure 2 was noticeably weaker than in
182 the CHO cell experiments (Figure 1). This is due to the methodology used in each experiment. In the
183 transduction experiments (Figure 1), cells were incubated with virus at 37°C for three hours. For studies
184 evaluating the role of sialic acid and HSPGs, cells were pre-treated with enzyme for one hour at 37°C.
185 Then virus was then incubated with cells on ice for one hour following enzymatic digestion to prevent
186 repair and reconstitution of the cleaved heparin/sialic acid. This incubation on ice (and for a shorter
187 period of time) likely decreases viral internalisation during the absorption step, seemingly more
188 profoundly for HAdV-C5/D49K than for the HAdV-C5 suggesting weaker binding at the cell surface or a
189 comparatively low frequency of cell surface receptor.

190 Desmoglein 2 (DSG2) is the other remaining well-established adenovirus receptor. DSG-2 is described to
191 interact with species BII adenovirus, including HAdV-B3K, via low affinity, avidity dependent
192 mechanism(34). We investigated whether HAdV-D49K might also interact with DSG2 by utilising surface
193 plasmon resonance (SPR), which we have previously used to establish a 66.9µM affinity between DSG2
194 and HAdV-D3K(35). HAdV-D49K had no detectable affinity for DSG2 (Figure 3A), an unsurprising finding
195 as DSG2 has never been observed as a receptor for any adenovirus outside of species B.

## 196 HAdV-D49 fiber knob can interact with CAR, but does not require it for cell entry

197 We also used SPR to further probe the binding affinity of HAdV-D49K, and a mutant version, HAdV-
198 D49.KO1.K, for CD46 and CAR. This HAdV-D49.KO1.K mutant, harbours the KO1 mutations S408E and
199 P409A in the fiber knob AB loop, previously shown to ablate CAR binding in HAdV-C5K(36). The structure
200 of the HAdV-D49.KO1.K fiber knob is also presented (Table 1, PDB 6QPO)(37). As predicted, we did not
201 observe binding between either fiber knob protein and CD46. However, we did observe HAdV-D49K
202 binding to CAR with a detectable 0.19µM affinity which was ablated by the KO1 mutation (Figure 3A).

203 We performed $IC_{50}$ binding studies using recombinant HAdV-D49K protein on CHO-CAR and CHO-BC1
204 cells and assessed the ability of the recombinant fiber knob protein to inhibit the binding of anti-CAR or
205 CD46 antibodies, respectively (Figure 3B). HAdV-D49K was able to block anti-CAR antibody binding to
206 CHO-CAR cells in a dose dependent manner ($IC_{50}$ = 0.16µg/$10^5$ cells, Figure 3B). However, no $IC_{50}$ could
207 be derived by using HAdV-D49K to block CD46 on CHO-BC1 cells, where HAdV-D49K was unable to
208 achieve more than 20% inhibition of antibody binding, suggesting weak or incidental CD46 interactions
209 (Figure 3B). Therefore, these data support the findings from SPR and transduction experiments that
210 HAdV-D49K may bind CAR with low affinity, but does not bind CD46.

211 Our earlier findings indicated that HAdV-C5/D49K is not dependent upon CAR for cell entry (Figure 1),
212 however our *in vitro* biological inhibition and SPR assays demonstrate CAR binding affinity (Figure 3A, B).

213 We further investigated this finding by performing transduction blocking experiments using the CAR
214 engaging HAdV-C5 and HAdV-C5/D49K with recombinant fiber knob protein of each virus in CHO-CAR
215 and CHO-K1 cells. As predicted, pre-incubation of CHO-CAR cells with recombinant HAdV-C5K efficiently
216 inhibited HAdV-C5 infection (Figure 3C), whilst blocking with HAdV-D49K inhibited infection by HAdV-C5
217 by approximately 50% (Figure 3D). Infecting CHO-CAR cells with HAdV-C5/D49K pseudotype and
218 attempting to block using HAdV-C5K (Figure 3E) or HAdV-D49K (Figure 3F) did not significantly inhibit
219 transduction efficiency. Finally, infection of CHO-K1 cells by HAdV-C5/D49K and blocking with HAdV-C5K
220 did not significantly inhibit transduction efficiency (Figure 3G), whilst blocking with HAdV-D49K reduced
221 transduction efficiency by approximately 50% (Figure 3H).

222 These data confirm that HAdV-D49K is capable of binding to CAR, albeit at approximately 1000x lower
223 affinity than HAdV-C5(35), but in a manner able to inhibit HAdV-C5 binding. These data confirm HAdV-
224 C5/D49K is capable of entering cells though a non-CAR mediated pathway, since HAdV-C5K cannot
225 inhibit HAdV-C5/D49K transduction in CHO-CAR cells (Figure 3E). Interestingly, HAdV-C5/D49K was able
226 to inhibit its own viral infection only in the absence of CAR (Figure 3H).

227 One potential explanation for this activity is that the unknown alternative receptor to CAR has a lower
228 affinity for HAdV-D49K than CAR. Therefore, in the presence of CAR the recombinant fiber knob would
229 be sequestered on the higher affinity CAR receptor leaving the alternative receptor free to interact with
230 the virus. A low affinity receptor would also, likely, depend upon avidity, so might not be observed with
231 single trimers of HAdV-D49K; a similar effect has previously been observed with HAdV-B3K and
232 DSG2(38) and CD46(39). This is supported by the observation what HAdV-D49K cannot transduce cells as
233 efficiently when incubated on ice in the absence of CAR, while HAdV-C5 and HAdV-C5/B35K, which form
234 high affinity receptor interactions, are unencumbered (Figure 2).

235 **HAdV-D49K may bind cells through a charge dependent mechanism**

236 To investigate other closely related HAdV with homologous fiber-knob proteins we performed a BLASTp
237 search using the HAdV-D49K amino acid sequence. This search revealed that the HAdV-D30K protein is
238 highly homologous to HAdV-D49K, differing in just 4 amino acid residues (Figure 4A).

239 We solved the crystal structures of HAdV-D30K (Figure 4B) and HAdV-D49K (Figure 4C). Diffraction data
240 collection statistics for these structures are provided in Table 1. We demonstrate that structurally,
241 HAdV-D30K and HAdV-D49K are highly homologous (RMSD = 0.292$Å^2$). Residue 338 is not surface
242 exposed on either fiber knob protein and is likely to be functionally homologous (HAdV-D49 =
243 Isoleucine338, HAdV-D30 = Valine338). However, the remaining 3 residue differences, E339K, G331A,
244 and Q332K (HAdV-D30K → D49K) are surface exposed at the apex of each fiber knob monomer (Figure
245 4D, E). The E339K and Q332K substitutions have opposing charges.

246 We investigated the transduction efficiency of HAdV-C5/D30K compared to HAdV-C5/D49K, HAdV-C5,
247 HAdV-C5.KO1, and HAdV-C5/D49.KO1.K in CHO-CAR (Figure 4F) and CHO-K1 cells (Figure 4G). HAdV-C5
248 infected CHO-CAR cells efficiently whilst the CAR-binding ablated KO1 mutant version did not, whilst
249 HAdV-C5/49K and the corresponding mutant HAdV-C5/49KO1.K infected CHO-CAR cells with similar
250 efficiency as observed for HAdV-C5/D49K in Figure 1A. HAdV-C5/D30K infected CHO-CAR cells with
251 approximately 40% efficiency (Figure 4F). In CHO-K1 cells HAdV-C5/D49K and the KO1 mutant were the
252 only viruses which achieved efficient transduction. Surprisingly, given the high homology to HAdV-
253 C5/D49K, the HAdV-C5/D30K pseudotype was inefficient in transducing CHO-K1 cells (<5% $GFP^+$, Figure
254 4G).

255 This profound difference in transduction efficiency between HAdV-C5/D30K and HAdV-C5/D49K must be
256 dependent upon the 3 surface exposed amino acid differences. We investigated the effect of the
257 opposing charges at residue substitutions 339 and 332 (Figure 4A-E) by modelling the electrostatic

258 surface potential of the two fiber knob proteins, based on our crystal structures (Figure 5). The surface
259 potential maps reveal that whilst structural homology was high, they present radically different
260 electrostatic surface potential distributions. HAdV-D30K is significantly more acidic (pI = 5.57) than
261 HAdV-D49K (pI = 8.26) (Figure 5).

262 Thus, it seems probable that the interaction with the unknown cell surface receptor requires basic
263 electrostatic potential. This is commensurate with the previous inference that its receptor is likely to be
264 low affinity, as electrostatic interfaces are often observed to be less stable than their ionic counterparts.
265 It is possible that the electrostatic potential differences explain the reduced transduction affinity
266 observed in HAdV-C5/D30K compared to HAdV-C5/D49K in CHO-CAR cells. Should the strong charge on
267 HAdV-D49K be opposed to that on the surface of CAR, this could enhance the interaction stability and
268 therefore overall virus affinity. It seems unlikely that the residue substitutions themselves would
269 strongly influence CAR affinity as they occur at the apex of the fiber knob, an area which is not critical
270 the CAR interface(1).

## 271 HAdV-C5/D49K is able to efficiently infect a large range of cancer cell lines

272 Given HAdV-C5/D49K infects cells independently of known adenovirus receptors we hypothesised that it
273 may form the basis of an efficient vector for cancer virotherapy applications. We therefore compared its
274 transduction efficiency to that of HAdV-C5 in panels of pancreatic, breast, oesophageal, colorectal,
275 ovarian and lung cancer cell lines (Table 2).

276 In pancreatic cancer cell lines HAdV-C5/D49K was consistently more efficient at cellular transduction
277 than HAdV-C5. This improved activity ranged between 4.2x more efficient in MiaPaCa2 cells to 210.9x
278 more efficient in BxPc3 cells. The most effectively transduced cell line was Panc10 cells, producing
279 $7.2x10^6$ RLU/mg of fluorescence, compared to the least efficient at just $4.0x10^5$ RLU/mg in Panc0403
280 cells. This suggests that the large differences between HAdV-C5/D49K and HAdV-C5 transduction levels

281 are likely due to the variability in the expression of CAR. A similarly broad range of different relative
282 infection efficiencies were observed in the breast cancer cell lines studied. In MCF7 cells and BT20 cells
283 HAdV-C5/D49K was nearly 500-fold more efficient at transducing the cells due to these cells expressing
284 low levels of CAR, with consequent poor levels of HAdV-C5 mediated transduction (Table 2).

285 DLD-1 colorectal cancer cells were efficiently transduced by both HAdV-C5 and HAdV-C5/D49K vectors,
286 at $5.0x10^6$ and $6.0x10^6$ RLU/mg respectively. This is the only cell line where no significant difference in
287 infectivity was observed. A427 lung carcinoma cells are the only line where HAdV-C5 mediated cellular
288 transduction was more efficient than HAdV-C5/D49K (0.6x). Whilst HAdV-C5/D49K transduced A427 cell
289 very efficiently ($7.2x10^6$ RLU/mg) HAdV-C5 achieved unusually high transduction efficiency ($1.2x10^7$
290 RLU/mg) (Table 2). Therefore, this result is not due to inefficient HAdV-C5/D49K transduction, but
291 unusually efficient HAdV-C5 transduction.

## 292 Conclusions

293 Previous experiments using whole HAdV-D49 virus concluded that it utilises CD46 as its primary cellular
294 receptor(23). The data described, generated using either purified HAdV-D49 fiber knob protein or a
295 pseudotyped HAdV-C5/D49K vector, clearly demonstrate CD46 to be implausible as a receptor for HAdV-
296 D49.

297 We demonstrate that the HAdV-D49 fiber knob has a weak affinity for CAR, although it is not dependent
298 upon this interaction to mediate efficient cell entry, and in fact the presence of CAR may inhibit cellular
299 transduction. In support of this we show a mutant vector, HAdV-C5/D49.KO1.K, containing mutations
300 within the fiber knob domain which ablate CAR affinity, retained the ability to efficiently transduce cells
301 in the absence of any detectable binding to CAR. Based on the low efficiency by which HAdV-C5/D49K
302 transduced cells when absorbed on ice and the observation that HAdV-D49K is only capable of inhibiting

303 HAdV-C5/D49K transduction in the absence of CAR, we tentatively suggest that the unknown receptor is
304 likely to be bound with weak affinity and virus attachment may be avidity dependent.

305 Regardless of the mechanism of interaction this study strongly suggests there is an as yet unknown
306 adenovirus receptor or mechanism of cell entry which mediates efficient transduction of a broad range
307 of cell lines. This is demonstrated by its ability to efficiently infect every cell line tested, throughout this
308 study. The weakest observed transduction was in Panc0403 cells where it achieved $4.0 \times 10^5$ RLU/mg of
309 luminescence. Whilst this is not a particularly strong transduction efficiency, it is still significantly higher
310 (33.0x, $P<0.05$) than that of HAdV-C5. It is likely, therefore, that the HAdV-C5/D49K vector described
311 here may be useful in biotechnology applications to efficiently express proteins in difficult to transduce
312 cell lines.

313 HAdV-C5/D49K represents a highly efficient gene transfer vehicle which is not restricted by any known
314 adenovirus tropism. It possesses a broad range of infectivity and has potential as both a laboratory
315 reagent, for the transient expression of transgenes, and as a therapeutic vaccine or oncolytic virus. For
316 oncolytic applications, it is likely that further refinement, such as the introduction of mutations known
317 to confer tumour selective replication, such as dl24 mutation(40–42) or the use of tumour specific
318 promoters such as hTERT(43) or survivin(44) to drive transgene therapeutic expression selectively within
319 tumour cells will be necessary to ensure tight tumour selectivity.

320 # Materials and Methods

321 **GFP transduction assay**

322 Adherent cells were seeded into a Nunc delta surface 96-well cell culture plate (ThermoFisher) at a
323 density of $5x10^4$ cells/well in 200µl of cell culture media and left to adhere overnight at 37˚C in a 5% $CO_2$
324 humidified atmosphere. Media was removed and cells washed twice with 200µl of PBS. Virus was added
325 at the desired concentration in 200µl of serum free RMPI 1640 and incubated for 3hrs. The virus
326 containing media was then removed and replaced with complete cell culture media and the cells
327 incubated for a further 45hrs. Cell culture media was then removed, the cells washed twice with 200µl
328 of PBS, trypsinised in 50µl of 0.05% Trypsin-EDTA (Gibco), and dissociated by pipetting. The trypsinised
329 cells were transferred to a 96-well V-bottom plate (ThermoFisher), neutralised with 100µl of complete
330 cell culture media, and pelleted by centrifugation at 1200RPM for 3mins. Supernatant was removed, the
331 cells washed once in 200µl of PBS, and resuspended in 100µl of 2% PFA (PBS containing 2% w/v
332 paraformaldehyde) and incubated at 4˚C for 15mins. Cells were again pelleted, washed twice in 200µl
333 PBS, then resuspended in 200µl PBS prior to analysis by flowcytometry.

334 Samples were analysed by flow cytometry on Attune NxT (ThermoFisher), voltages were set prior to
335 each experiment, for each cell type, using an uninfected cell population treated identically. Data was
336 analysed using FlowJo v10 (FlowJo, LLC), gating sequentially on singlets, cell population, and GFP
337 positive cells. Levels of infection were defined as the percentage of GFP positive cells (% +ve), and/or
338 Total Fluorescence (TF), defined as the percentage of GFP positive cells multiplied by the median
339 fluorescent intensity (MFI) of the GFP positive population. These measures are distinct in that % +ve
340 describes the total proportion of cells infected, and TF describes the total efficiency of transgene
341 delivery.

342 **Luciferase transduction assay**

343 Luciferase infectivity assays were performed using the luciferase assay system kit (Promega). Cells were
344 seeded into a Nunc delta surface 96-well cell culture plate (ThermoFisher) at a density of $2x10^4$
345 cells/well in 200µl of cell culture media and left to adhere overnight at 37˚C in a 5% $CO_2$ humidified
346 atmosphere. Media was removed and cells washed once with 200µl of PBS. Luciferase transgene
347 encoding replication incompetent viruses were added to the wells at the required titre in 200µl of serum
348 free RMPI 1640 and incubated for 3hrs. The virus containing media was then removed and replaced with
349 complete cell culture media and the cells incubated for a further 45hrs. Cell culture media was then
350 removed, the cells washed twice with 200µl of PBS, and were then lysed in 100µl of cell culture lysis
351 buffer (part of the Promega kit) diluted to 1x in $ddH_2O$. The plate was then frozen at -80˚C.

352 After thaw, 10µl of lysate from the cell culture plate mixed then was transferred to a white Nunc 96-
353 microwell plate (ThermoFisher) and 100µl of luciferase assay reagent (Promega Kit) added. Luciferase
354 activity was then measured in relative light units (RLU) by plate reader (Clariostar, BMG Labtech). Total
355 protein concentration was determined in the lysate using the Pierce BCA protein assay kit
356 (Thermofisher) according to the manufacturers protocol, absorbance was measured on an iMark
357 microplate absorbance reader (BioRad).

358 Relative virus infection was determined by normalising the measured luciferase intensity to the total
359 protein concentration (RLU was divided by protein concentration). This gave a final infectivity readout in
360 RLU/mg of protein.

361 **Blocking of virus infection with recombinant fiber knob protein**

362 This assay was also performed using the luciferase assay system kit (Promega). Cells were seeded into a
363 Nunc delta surface 96-well cell culture plate (ThermoFisher) at a density of $2x10^4$ cells/well in 200µl of
364 cell culture media and left to adhere overnight at 37˚C in a 5% $CO_2$ humidified atmosphere. Media was

365 removed and cells washed 2x with 200µl of cold PBS and the plate cooled on ice. 20pg/cell of
366 recombinant adenovirus fiber knob was added to each well in 200µl of cold PBS and incubated on ice in
367 a 4˚C cold room for 1hr. Media was then removed and luciferase transgene encoding replication
368 incompetent viruses added to the necessary wells at the required titre in 200µl of cold serum free RMPI
369 1640 and incubated on ice in a 4˚C cold room for 1hr. The virus containing media was then removed and
370 replaced with complete cell culture media and the cells incubated for a further 45hrs under normal cell
371 culture conditions. From this point forward the assay is identical to the GFP and luciferase transduction
372 assays.

373 **Heparinase and Neuraminidase transduction assays**

374 Cells were seeded at a density of $5x10^4$ cells/well in a flat bottomed 96 well cell culture plate and
375 incubated overnight at 37°C to adhere. Cells were washed twice with 200µl of PBS. 50µl of
376 neuraminidase (from Vibrio Cholera, Merk) at a concentration of 50mU/ml, or 50µl of Heparinase III
377 (from Flavobacterium heparinum, Merck) at a concentration of 1U/ml was diluted in serum free media,
378 added to the appropriate wells, and incubated for 1hr at 37°C. Cells were cooled on ice and washed
379 twice with 200µl of PBS. Green Fluorescent Protein (GFP) expressing, replication incompetent viruses
380 were added to the appropriate wells at a concentration of 5000 viral particles per cell, in 100µl of serum
381 free media, at 4°C, and incubated on ice for 1hr. Serum free media alone was added to uninfected
382 control wells. Cells were washed twice with 200µl of cold PBS, complete media added (DMEM, 10% FCS)
383 and incubated for a further 48hrs at 37°C. Cells were then trypsinised and transferred to a 96 well V-
384 bottom plate, washed twice in 200µl of PBS and fixed in 2% paraformaldehyde containing PBS for
385 20mins before wash, and resuspension in 200µl of PBS.

386 Samples were analysed by flow cytometry on Attune NxT (ThermoFisher), voltages were set prior to
387 each experiment, for each cell type, using an uninfected cell population treated identically. Data was

388 analysed using FlowJo v10 (FlowJo, LLC), gating sequentially on singlets, cell population, and GFP
389 positive cells. Levels of transdcution were defined as the percentage of GFP positive cells (% +ve), and/or
390 Total Fluorescence (TF), defined as the percentage of GFP positive cells multiplied by the median
391 fluorescent intensity (MFI) of the GFP positive population. These measures are distinct in that % +ve
392 describes the total proportion of cells infected, and TF describes the total efficiency of transgene
393 delivery.

394 **Surface Plasmon Resonance**

395 Surface plasmon resonance was performed, in triplicate, as previously described, using recombinant
396 HAdV-D49K protein(35). Approximately 5000 RU of Recombinant Human Desmoglein-2 Fc Chimera
397 Protein (R&D Systems, Catalogue number 947-DM-100) was amine coupled to a CM5 sensor chip at a
398 slow flow-rate of 10 µl/min to ensure uniform distribution on the chip surface.

399 **Competition Inhibition Assay**

400 Competition inhibition assays of antibody binding to cell surface receptors were performed as previously
401 described(35).

402 **Generation of recombinant fiber knob proteins**

403 Recombinant fiber knob proteins used in transduction inhibition, antibody blocking, and crystallisation
404 experiments were produced as previous described(24, 35). Briefly, pQE-30 vectors containing the
405 sequence of the relevant fiber knob protein, spanning from 13 amino acids preceding the TLW motif to
406 the stop codon, were transformed into SG13009 E.coli harbouring the pREP-4 plasmid. 1L of these E.coli
407 were grown to OD0.6 and protein expression induced with a final concentration of 0.5mM IPTG. E.coli
408 were harvested by centrifugation and resuspended in 50ml lysis buffer (50 mM Tris, pH 8.0, 300 mM
409 NaCl, 1% (v/v) NP40, 1 mg/ml Lysozyme, 1 mM β-mercaptoethanol). Sample was then loaded onto a

410 HisTrap FF Crude column and eluted by imidazole. Fractions determined to contain protein of interest
411 were then concentrated to <1ml total volume and purified by size exclusion chromatography using a
412 Superdex 200 10/300 GL Increase column.

### 413 Fiber knob protein crystallisation and structure determination by X-Ray 414 crystallography

415 HAdV-D49K, HAdV-D49.KO1.K, and HAdV-D30K were crystallised in the same manner as previously
416 described(24, 35). Both HAdV-D49K and HAdV-D49.KO1.K crystals formed in 0.1M MMT, 25% w/v
417 PEG1500, whilst HAdV-D30K crystallised in 0.1M SPG, 25% w/v PEG 1500. All crystals formed in 2-7 days
418 in sitting drop format. Data collection statistics are described in Table 1 and the structures were solved
419 by molecular replacement using PDB 6FJN.

### 420 Calculation of electrostatic surface potentials and pIs

421 Electrostatic surface potential and isoelectric points were calculated at pH 7.2 using the PDB2PQR Server
422 (V 2.1.1)(45) as previous described(24).

### 423 RMSD calculation, sequence alignment, and imaging of crystal structures

424 Alignments were performed using the Clustal Omega multiple sequence alignment algorithm and
425 visualised with BioEdit(46, 47). RMSD calculations were performed using the 'align' command in PyMOL
426 2.0, which was also used to visualise protein structures(48).

## 427 Acknowledgements

428 ATB was funded by a Tenovus Cancer Care PhD studentship (reference PhD2015/L13) to ALP. GM was
429 supported by a Cancer Research UK ECMC centre award (C7838/A25173). JAD is funded by a Cancer
430 Research UK Biotherapeutic Programme award (reference C52915/A29104) to ALP. EM is supported by a

Wellcome Trust ISSF Translational Kickstarter Award (reference 517732) to ALP. RMM was supported by the Cardiff University Research Opportunities Placement (CUROP) to ALP. PJR and ALP are funded by HEFCW. The authors acknowledge the Diamond Light Source for beamtime (proposal MX18812) and the staff of beamline I03 for assistance with diffraction data collection. The authors acknowledge Johanne Pentier for technical assistance with SPR data collection, as well as Aaron Wall and Anna Fuller for assistance with FPLC.

437 # References


438 1. Baker AT, Aguirre-Hernández C, Halldén G, Parker AL. 2018. Designer Oncolytic Adenovirus:
439 Coming of Age. Cancers 10:201.

440 2. Russell WC. 2009. Adenoviruses: update on structure and function. J Gen Virol 90:1–20.

441 3. Stanton RJ, McSharry BP, Armstrong M, Tomasec P, Wilkinson GWG. 2008. Re-engineering
442 adenovirus vector systems to enable high-throughput analyses of gene function. BioTechniques
443 45:659–662, 664–668.

444 4. Alba R, Baker AndrewH, Nicklin StuartA. 2012. Vector Systems for Prenatal Gene Therapy:
445 Principles of Adenovirus Design and Production, p. 55–84. *In* Coutelle, C, Waddington, SN (eds.),
446 Prenatal Gene Therapy. Humana Press.

447 5. Weaver EA, Barry MA. 2013. Low Seroprevalent Species D Adenovirus Vectors as Influenza
448 Vaccines. PLOS ONE 8:e73313.

449 6. Atasheva S, Yao J, Shayakhmetov DM. 2019. Innate immunity to adenovirus: lessons from mice.
450 FEBS Lett 593:3461–3483.

451 7. Ahi YS, Bangari DS, Mittal SK. 2011. Adenoviral Vector Immunity: Its Implications and
452 circumvention strategies. Curr Gene Ther 11:307–320.

453 8. Dakin RS, Parker AL, Delles C, Nicklin SA, Baker AH. 2015. Efficient transduction of primary vascular
454 cells by the rare adenovirus serotype 49 vector. Hum Gene Ther 26:312–319.

455 9. Abbink P, Lemckert AAC, Ewald BA, Lynch DM, Denholtz M, Smits S, Holterman L, Damen I, Vogels
456 R, Thorner AR, O'Brien KL, Carville A, Mansfield KG, Goudsmit J, Havenga MJE, Barouch DH. 2007.

457 Comparative Seroprevalence and Immunogenicity of Six Rare Serotype Recombinant Adenovirus
458 Vaccine Vectors from Subgroups B and D. J Virol 81:4654–4663.

459 10. Zhao H, Xu C, Luo X, Wei F, Wang N, Shi H, Ren X. 2018. Seroprevalence of Neutralizing Antibodies
460 against Human Adenovirus Type-5 and Chimpanzee Adenovirus Type-68 in Cancer Patients. Front
461 Immunol 9.

462 11. Teigler JE, Iampietro MJ, Barouch DH. 2012. Vaccination with Adenovirus Serotypes 35, 26, and 48
463 Elicits Higher Levels of Innate Cytokine Responses than Adenovirus Serotype 5 in Rhesus Monkeys.
464 J Virol 86:9590–9598.

465 12. Dyer A, Di Y, Calderon H, Illingworth S, Kueberuwa G, Tedcastle A, Jakeman P, Chia SL, Brown A,
466 Silva MA, Barlow D, Beadle J, Hermiston T, Ferguson DJ, Champion B, Fisher KD, Seymour LW.
467 2017. Oncolytic Group B Adenovirus Enadenotucirev Mediates Non-apoptotic Cell Death with
468 Membrane Disruption and Release of Inflammatory Mediators. Mol Ther Oncolytics 4:18–30.

469 13. Di Y, Seymour L, Fisher K. 2014. Activity of a group B oncolytic adenovirus (ColoAd1) in whole
470 human blood. Gene Ther 21:440–443.

471 14. 2009. Human adenovirus B strain ColoAd1, complete genome.

472 15. Long-term Safety Follow-up of Participants Exposed to the Candidate Ebola Vaccines Ad26.ZEBOV
473 and/or MVA-BN-Filo - Full Text View - ClinicalTrials.gov.

474 16. A Study to Assess Ebola Vaccines ChAd3-EBO-Z and Ad26.ZEBOV - Full Text View -
475 ClinicalTrials.gov.

476 17. Vogels R, Zuijdgeest D, Rijnsoever R van, Hartkoorn E, Damen I, Béthune M-P de, Kostense S,
477 Penders G, Helmus N, Koudstaal W, Cecchini M, Wetterwald A, Sprangers M, Lemckert A, Ophorst

478 O, Koel B, Meerendonk M van, Quax P, Panitti L, Grimbergen J, Bout A, Goudsmit J, Havenga M.
479 2003. Replication-Deficient Human Adenovirus Type 35 Vectors for Gene Transfer and Vaccination:
480 Efficient Human Cell Infection and Bypass of Preexisting Adenovirus Immunity. J Virol 77:8263–
481 8271.

482 18. Schnurr D, Dondero ME. 1993. Two New Candidate Adenovirus Serotypes. Intervirology 36:79–83.

483 19. De Jong JC, Wermenbol AG, Verweij-Uijterwaal MW, Slaterus KW, Wertheim-Van Dillen P, Van
484 Doornum GJJ, Khoo SH, Hierholzer JC. 1999. Adenoviruses from Human Immunodeficiency Virus-
485 Infected Individuals, Including Two Strains That Represent New Candidate Serotypes Ad50 and
486 Ad51 of Species B1 and D, Respectively. J Clin Microbiol 37:3940–3945.

487 20. Ishiko H, Shimada Y, Konno T, Hayashi A, Ohguchi T, Tagawa Y, Aoki K, Ohno S, Yamazaki S. 2008.
488 Novel Human Adenovirus Causing Nosocomial Epidemic Keratoconjunctivitis. J Clin Microbiol
489 46:2002–2008.

490 21. 2016. Human adenovirus 49 gene for fiber protein, partial cds, strain: T87-677.

491 22. Al Qurashi YMA, Alkhalaf MA, Lim L, Guiver M, Cooper RJ. 2012. Sequencing and phylogenetic
492 analysis of the hexon, fiber, and penton regions of adenoviruses isolated from AIDS patients. J Med
493 Virol 84:1157–1165.

494 23. Lemckert AAC, Grimbergen J, Smits S, Hartkoorn E, Holterman L, Berkhout B, Barouch DH, Vogels
495 R, Quax P, Goudsmit J, Havenga MJE. 2006. Generation of a novel replication-incompetent
496 adenoviral vector derived from human adenovirus type 49: manufacture on PER.C6 cells, tropism
497 and immunogenicity. J Gen Virol 87:2891–2899.

498 24. Baker AT, Mundy RM, Davies JA, Rizkallah PJ, Parker AL. 2019. Human adenovirus type 26 uses
499 sialic acid–bearing glycans as a primary cell entry receptor. Sci Adv 5:eaax3567.

500 25. Gaggar A, Shayakhmetov DM, Lieber A. 2003. CD46 is a cellular receptor for group B adenoviruses.
501 Nat Med 9:1408–1412.

502 26. Roelvink PW, Lizonova A, Lee JGM, Li Y, Bergelson JM, Finberg RW, Brough DE, Kovesdi I, Wickham
503 TJ. 1998. The Coxsackievirus-Adenovirus Receptor Protein Can Function as a Cellular Attachment
504 Protein for Adenovirus Serotypes from Subgroups A, C, D, E, and F. J Virol 72:7909–7915.

505 27. Shayakhmetov DM, Lieber A. 2000. Dependence of Adenovirus Infectivity on Length of the Fiber
506 Shaft Domain. J Virol 74:10274–10286.

507 28. Alba R, Bradshaw AC, Mestre-Francés N, Verdier J-M, Henaff D, Baker AH. 2012. Coagulation factor
508 X mediates adenovirus type 5 liver gene transfer in non-human primates (*Microcebus murinus*).
509 Gene Ther 19:109–113.

510 29. Alba R, Bradshaw AC, Parker AL, Bhella D, Waddington SN, Nicklin SA, van Rooijen N, Custers J,
511 Goudsmit J, Barouch DH, McVey JH, Baker AH. 2009. Identification of coagulation factor (F)X
512 binding sites on the adenovirus serotype 5 hexon: effect of mutagenesis on FX interactions and
513 gene transfer. Blood 114:965–971.

514 30. Parker AL, Waddington SN, Nicol CG, Shayakhmetov DM, Buckley SM, Denby L, Kemball-Cook G, Ni
515 S, Lieber A, McVey JH, Nicklin SA, Baker AH. 2006. Multiple vitamin K-dependent coagulation
516 zymogens promote adenovirus-mediated gene delivery to hepatocytes. Blood 108:2554–2561.

517 31. Waddington SN, McVey JH, Bhella D, Parker AL, Barker K, Atoda H, Pink R, Buckley SMK, Greig JA,
518 Denby L, Custers J, Morita T, Francischetti IMB, Monteiro RQ, Barouch DH, Rooijen N van, Napoli C,

519 Havenga MJE, Nicklin SA, Baker AH. 2008. Adenovirus Serotype 5 Hexon Mediates Liver Gene
520 Transfer. Cell 132:397–409.

521 32. Burmeister WP, Guilligay D, Cusack S, Wadell G, Arnberg N. 2004. Crystal Structure of Species D
522 Adenovirus Fiber Knobs and Their Sialic Acid Binding Sites. J Virol 78:7727–7736.

523 33. Arnberg N, Edlund K, Kidd AH, Wadell G. 2000. Adenovirus Type 37 Uses Sialic Acid as a Cellular
524 Receptor. J Virol 74:42–48.

525 34. Vassal-Stermann E, Effantin G, Zubieta C, Burmeister W, Iseni F, Wang H, Lieber A, Schoehn G,
526 Fender P. 2019. CryoEM structure of adenovirus type 3 fibre with desmoglein 2 shows an unusual
527 mode of receptor engagement. Nat Commun 10:1181.

528 35. Baker AT, Greenshields-Watson A, Coughlan L, Davies JA, Uusi-Kerttula H, Cole DK, Rizkallah PJ,
529 Parker AL. 2019. Diversity within the adenovirus fiber knob hypervariable loops influences primary
530 receptor interactions. Nat Commun 10:741.

531 36. Smith T, Idamakanti N, Kylefjord H, Rollence M, King L, Kaloss M, Kaleko M, Stevenson SC. 2002. In
532 Vivo Hepatic Adenoviral Gene Delivery Occurs Independently of the Coxsackievirus–Adenovirus
533 Receptor. Mol Ther 5:770–779.

534 37. Jakubczak JL, Rollence ML, Stewart DA, Jafari JD, Seggern DJV, Nemerow GR, Stevenson SC,
535 Hallenbeck PL. 2001. Adenovirus Type 5 Viral Particles Pseudotyped with Mutagenized Fiber
536 Proteins Show Diminished Infectivity of Coxsackie B-Adenovirus Receptor-Bearing Cells. J Virol
537 75:2972–2981.

538 38. Vassal-Stermann E, Mottet M, Ducournau C, Iseni F, Vragniau C, Wang H, Zubieta C, Lieber A,
539 Fender P. 2018. Mapping of Adenovirus of serotype 3 fibre interaction to desmoglein 2 revealed a
540 novel 'non-classical' mechanism of viral receptor engagement. Sci Rep 8.

541 39. Trinh HV, Lesage G, Chennamparampil V, Vollenweider B, Burckhardt CJ, Schauer S, Havenga M,
542 Greber UF, Hemmi S. 2012. Avidity Binding of Human Adenovirus Serotypes 3 and 7 to the
543 Membrane Cofactor CD46 Triggers Infection. J Virol 86:1623–1637.

544 40. Uusi-Kerttula H, Davies JA, Thompson J, Wongthida P, Evgin L, Shim KG, Bradshaw A, Baker AT,
545 Rizkallah PJ, Jones R, Hanna L, Hudson E, Vile R, Chester JD, Parker AL. 2018. Ad5NULL-A20 - a
546 tropism-modified, αvβ6 integrin-selective oncolytic adenovirus for epithelial ovarian cancer
547 therapies. Clin Cancer Res clincanres.1089.2018.

548 41. Loskog A, Maleka A, Mangsbo S, Svensson E, Lundberg C, Nilsson A, Krause J, Agnarsdottir M,
549 Sundin A, Ahlstrom H, Totterman TH, Ullenhag G. 2016. Immunostimulatory AdCD40L gene
550 therapy combined with low-dose cyclophosphamide in metastatic melanoma patients. Br J Cancer
551 114:872–80.

552 42. Man YKS, Davies JA, Coughlan L, Pantelidou C, Blázquez-Moreno A, Marshall JF, Parker AL, Halldén
553 G. 2018. The Novel Oncolytic Adenoviral Mutant Ad5-3Δ-A20T Retargeted to αvβ6 Integrins
554 Efficiently Eliminates Pancreatic Cancer Cells. Mol Cancer Ther 17:575–587.

555 43. Onimaru M, Ohuchida K, Nagai E, Mizumoto K, Egami T, Cui L, Sato N, Uchino J, Takayama K,
556 Hashizume M, Tanaka M. 2010. Combination with low-dose gemcitabine and hTERT-promoter-
557 dependent conditionally replicative adenovirus enhances cytotoxicity through their crosstalk
558 mechanisms in pancreatic cancer. Cancer Lett 294:178–86.

559 44. Wang W, Ji W, Hu H, Ma J, Li X, Mei W, Xu Y, Hu H, Yan Y, Song Q, Li Z, Su C. 2013. Survivin
560 promoter-regulated oncolytic adenovirus with Hsp70 gene exerts effective antitumor efficacy in
561 gastric cancer immunotherapy. Oncotarget 5:150–160.

562 45. Jurrus E, Engel D, Star K, Monson K, Brandi J, Felberg LE, Brookes DH, Wilson L, Chen J, Liles K, Chun
563 M, Li P, Gohara DW, Dolinsky T, Konecny R, Koes DR, Nielsen JE, Head-Gordon T, Geng W, Krasny R,
564 Wei G-W, Holst MJ, McCammon JA, Baker NA. 2018. Improvements to the APBS biomolecular
565 solvation software suite. Protein Sci Publ Protein Soc 27:112–128.

566 46. Sievers F, Wilm A, Dineen D, Gibson TJ, Karplus K, Li W, Lopez R, McWilliam H, Remmert M, Söding
567 J, Thompson JD, Higgins DG. 2011. Fast, scalable generation of high-quality protein multiple
568 sequence alignments using Clustal Omega. Mol Syst Biol 7:539–539.

569 47. Li W, Cowley A, Uludag M, Gur T, McWilliam H, Squizzato S, Park YM, Buso N, Lopez R. 2015. The
570 EMBL-EBI bioinformatics web and programmatic tools framework. Nucleic Acids Res 43:W580-4.

571 48. Schrödinger, LLC. The PyMOL Molecular Graphics System, Version 2.0.

572

573 **Figure Legends:**

574 **Figure 1: HAdV-C5/D49K infection is not dependent upon CAR or CD46.** Transduction assays were
575 performed in Chinese Hamster Ovary (CHO) cells stably expressing CAR (A), CHO-BC1 cells, stably
576 expressing human CD46 isoform BC1 (B), or CHO-K1 cells, which do not express any known adenovirus
577 fiber-knob receptors (C, D). Cells were infected with 5,000 viral particles per cell of replication deficient
578 HAdV-C5, HAdV-C5/B35K, or HAdV-C5/49K expressing a GFP transgene (A-C), or HAdV-C5, HAdV-C5/49K
579 or HAdV-C5/49F expressing luciferase (D). n=3 error is ±SD

580 **Figure 2: HAdV-C5/49K transduction is not dependent upon HSPGs, sialic acid bearing glycans or**
581 **Desmoglein 2 (DSG2).** Transduction assays were performed in CHO-K1 (A) or SKOV-3 (B) cells with and
582 without heparinase pre-treatment. As a positive control, HAdV-C5 assays also were performed also in
583 the presence of 10µg/ml of FX. Transduction assays were performed with the indicated viral vectors in
584 CHO-K1 (C) or SKOV-3 (D) cells which had been pre-treated with neuraminidase to cleave cell surface
585 sialic acid. Cells were infected with 5,000 viral particles per cell of replication deficient HAdV-C5, HAdV-
586 C5/B35K, or HAdV-C5/49K expressing a GFP transgene, n=3 error is ±SD. *= P<0.05, **= P<0.01, ***=
587 P<0.005, , ****= P<0.001.

588 **Figure 3: HAdV-D49K interacts with CAR but is not dependent upon it as an entry receptor.** Surface
589 plasmon resonance to detect potential interactions between HAdV-D49K or HAdV-D49.KO1.K and CAR,
590 CD46 and DSG2 (A). Antibody binding inhibition assays to assess the ability of recombinant HAdV-D49K
591 to inhibit antibody binding to CHO-CAR or CHO-BC1 cells (B). Blocking of HAdV-C5 mediated
592 transduction was studied by preincubation of CHO-CAR cells with HAdV-C5K (C) or HAdV-D49K (D).
593 Blocking of HAdV-C5/D49K mediated transduction was studied by preincubation of CHO-CAR cells with
594 HAdV-C5K (E) or HAdV-D49K (F). Blocking of HAdV-C5/D49K mediated transduction was studied by
595 preincubation of CHO-K1 cells with HAdV-C5K (G) or HAdV-D49K (H). Cells were infected with 5,000 viral

596 particles per cell of replication deficient HAdV-C5 or HAdV-C5/D49K expressing a luciferase transgene,
597 with and without blockade by 20µg of recombinant HAdV-C5 or HAdV-D49 fiber knob protein. n=3 error
598 is ±SD. *= P<0.05, **= P<0.01.

599 **Figure 4: HAdV-D49K differs from HAdV-D30K in only three surface exposed amino acids but**
600 **demonstrates radically altered cellular tropism.** Clustal Ω sequence alignment (numbering based on
601 whole fiber sequence) of HAdV-D30K and HAdV-D49K (A). Viewed from the apex down the three fold
602 axis, as if towards the viral capsid, the crystal structures of HAdV-D30K (B) and HAdV-D49K (C) reveal
603 that three of these residues are surface exposed. These residues can be seen projecting into the solvent
604 from loops on the apex of HAdV-D30K (D) and HAdV-D49K (E), residue numbers and names correspond
605 to the fiber-knob protein depicted in that frame. Sticks representing residues belonging to HAdV-D30K
606 and HAdV-D49K are seen in pink and green, respectively. Transduction assays were performed to assess
607 tropism of HAdV-C5/D30K, HAdV-C5/D49K and HAdV-C5/D49.KO1.K in CHO-CAR cells (F) and CHO-K1
608 cells (G). Cells were infected with 5,000 viral particles per cell of replication deficient HAdV-C5 or HAdV-
609 C5/D49K expressing a luciferase transgene, with and without blockade by 20µg of recombinant HAdV-C5
610 or HAdV-D49 fiber knob protein.

611 **Figure 5: The residue differences between HAdV-D30K and HAdV-D49K effect the surface electrostatic**
612 **potential of the fiber knob.** The calculated pI of HAdV-D30K and HAdV-D49K is differ as a result of the
613 residue changes, which are shown as green sticks as they occur in that fiber knob protein. The calculated
614 electrostatic surface potential at pH7.35 is projected on a -10mV to +10mV ramp (Red to Blue). HAdV-
615 D49K is seen to have much more basic potential around the apex where the residue substitutions are.

616 **Table 1:** Single crystal diffraction data collection statistics for fiber knob crystal structures determined in
617 this study.

618 **Table 2:** Comparison of transduction of various cancer cell lines by HAdV-C5 and HAdV-C5/D49K. *=

619 P<0.05, **=P<0.01, ***=P<0.001, ****=P<0.0001, ns=not significant.

620

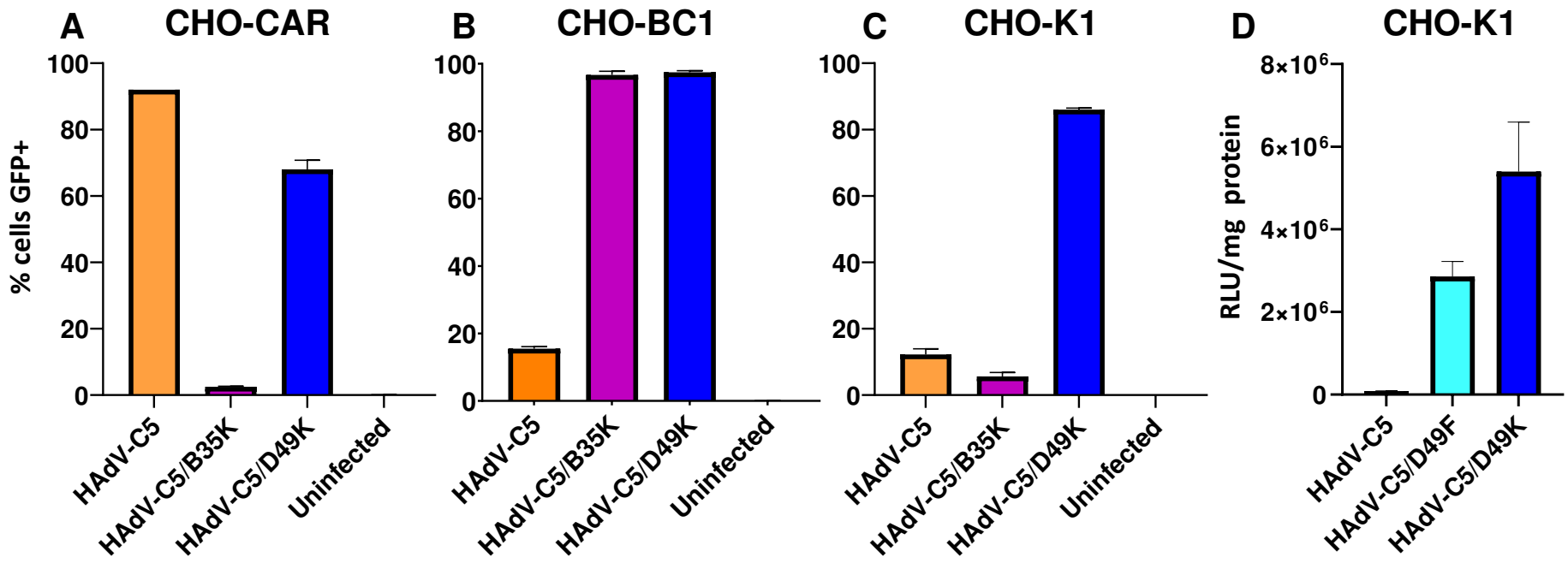
A
CHO-CAR
% cells GFP+
100
80
60
40
20
0
HAdV-C5
HAdV-C5/B35K
HAdV-C5/D49K
Uninfected
B
CHO-BC1
100
80
60
40
20
0
HAdV-C5
HAdV-C5/B35K
HAdV-C5/D49K
Uninfected
C
CHO-K1
100
80
60
40
20
0
HAdV-C5
HAdV-C5/B35K
HAdV-C5/D49K
Uninfected
D
CHO-K1
RLU/mg protein
8×10⁶
6×10⁶
4×10⁶
2×10⁶
0
HAdV-C5
HAdV-C5/D49F
HAdV-C5/D49K

Figure 1

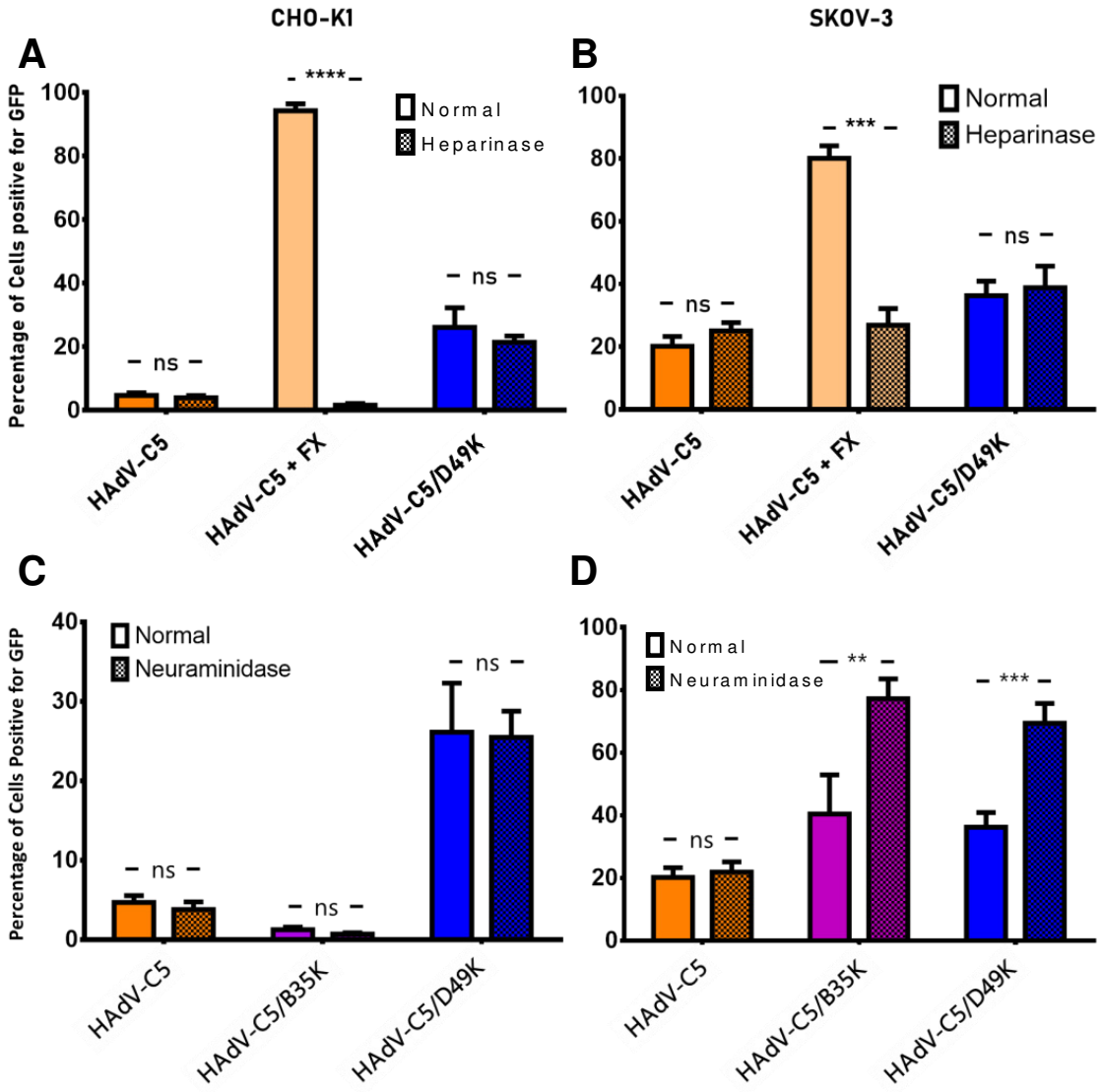
CHO-K1
SKOV-3
A
B
C
D
Percentage of Cells positive for GFP
Percentage of Cells Positive for GFP
Normal
Heparinase
Neuraminidase
ns
****
***
**
HAdV-C5
HAdV-C5 + FX
HAdV-C5/D49K
HAdV-C5/B35K

Figure 2

**A**

| | HAdV-D49K | | | HAdV-D49.KO1.K | | |
|---|---|---|---|---|---|---|
| | $K_{on}$ ($M^{-1}$ $s^{-1}$) | $K_{off}$ ($s^{-1}$) | $K_D$ ($\mu M$) | $K_{on}$ ($M^{-1}$ $s^{-1}$) | $K_{off}$ ($s^{-1}$) | $K_D$ ($\mu M$) |
| CAR | $6.1 \times 10^3$ | 0.0012 | 0.19 | nb | nb | No binding |
| CD46 | nb | nb | No binding | nb | nb | No binding |
| DSG2 | nb | nb | No binding | nb | nb | No binding |

nm = kinetics too fast to measure
nb = no binding

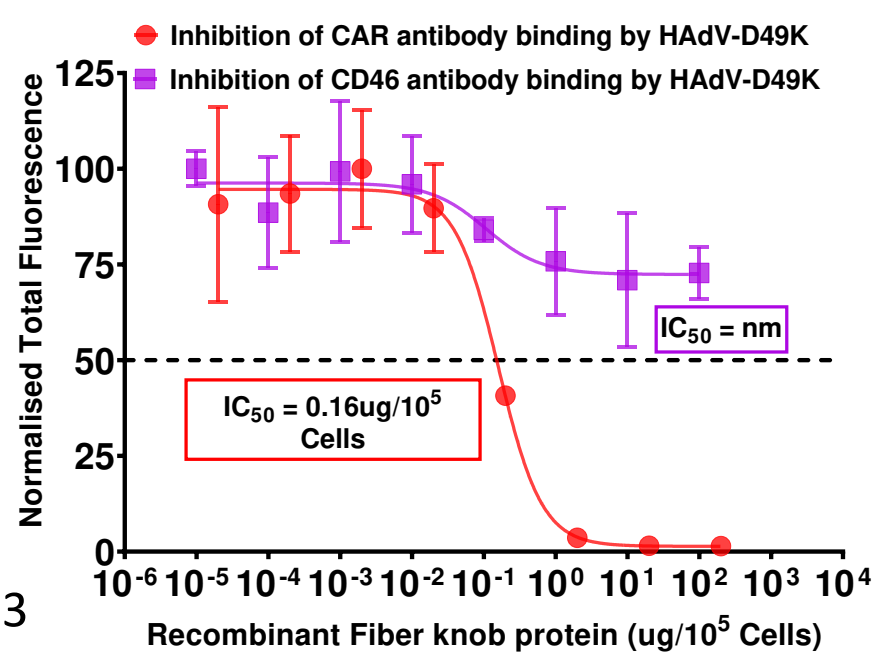


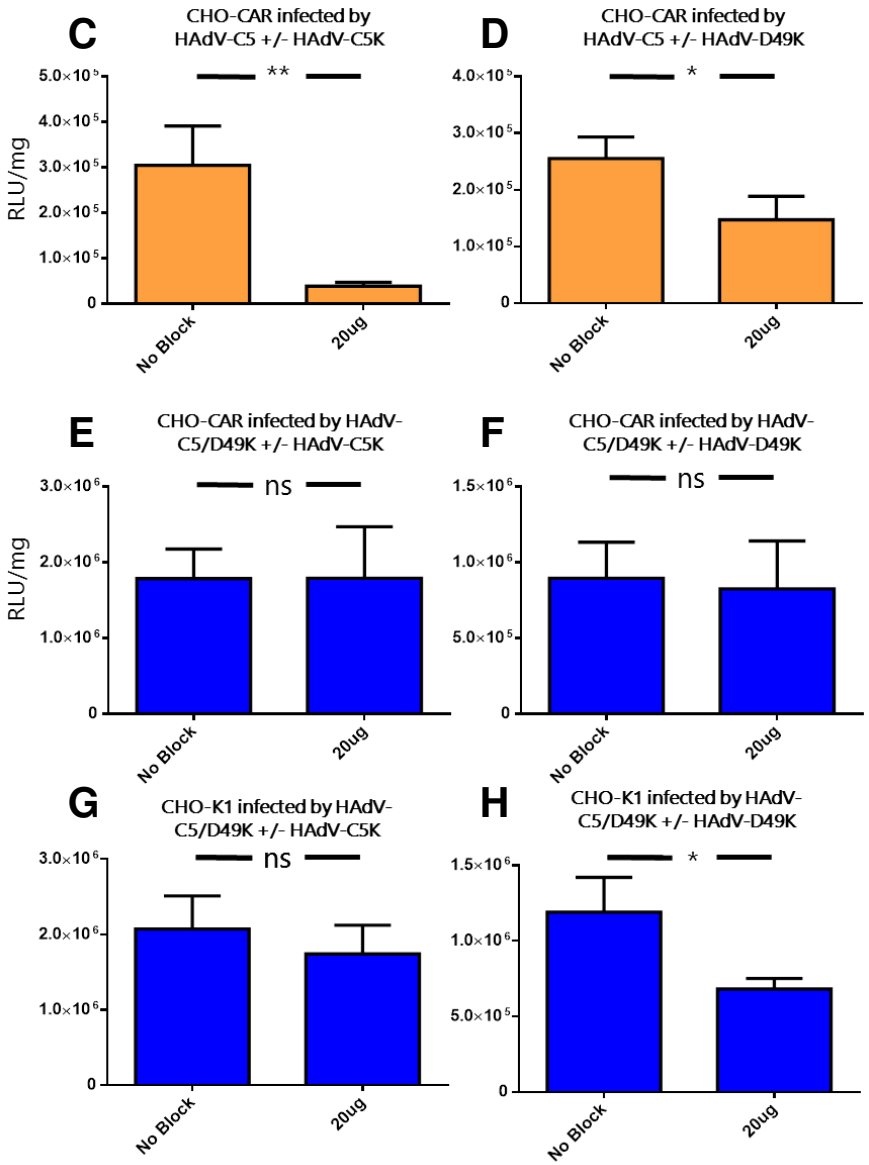


Figure 3

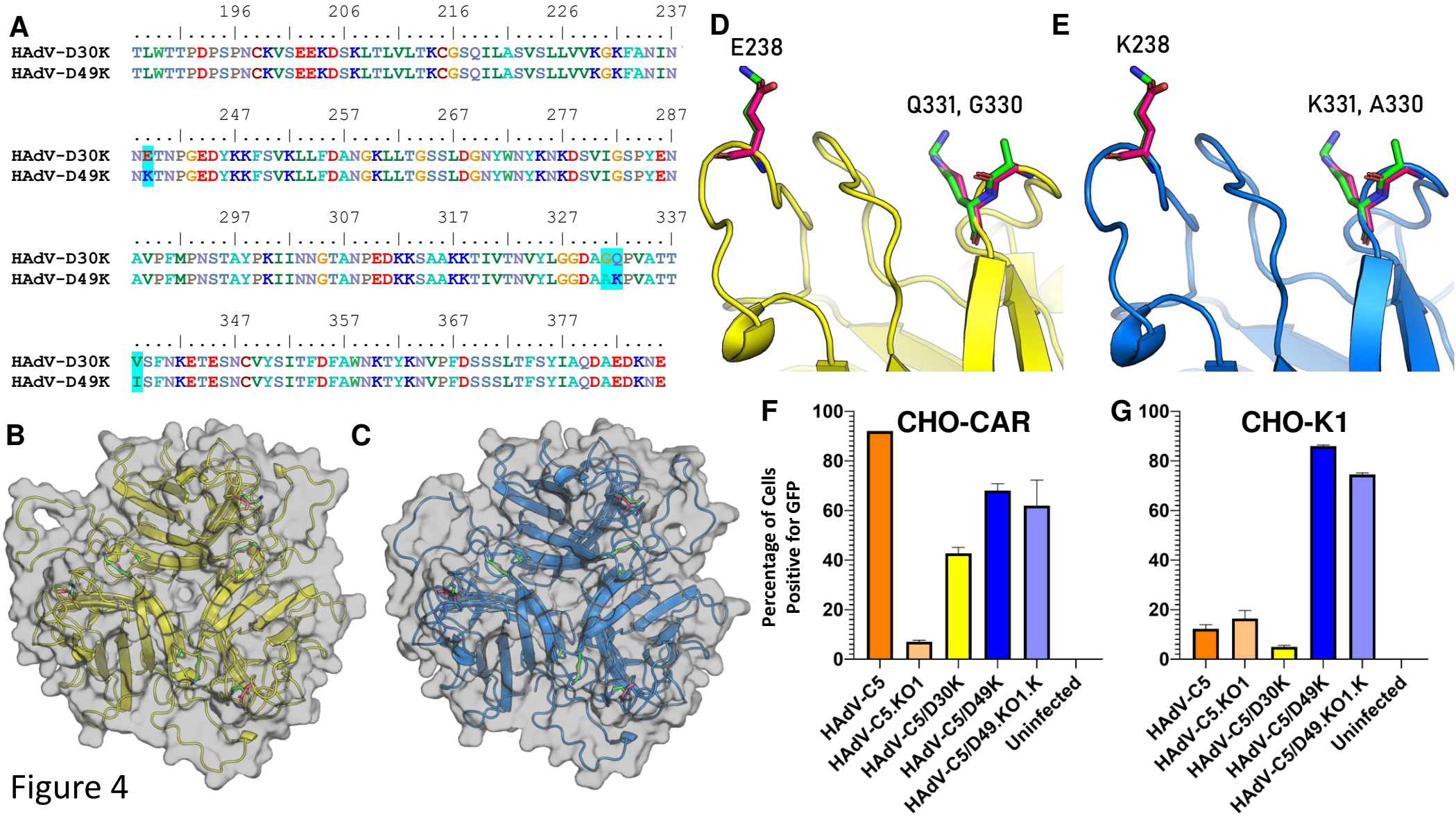
A
196 206 216 226 237
HAdV-D30K TLWTTPDPSPNCKVSEEKDSKLTLVLTKCGSQILASVSLLVVKGKFANIN
HAdV-D49K TLWTTPDPSPNCKVSEEKDSKLTLVLTKCGSQILASVSLLVVKGKFANIN
247 257 267 277 287
HAdV-D30K NETNPGEDYKKFSVKLLFDANGKLLTGSSLDGNYWNYKNKDSVIGSPYEN
HAdV-D49K NKTNPGEDYKKFSVKLLFDANGKLLTGSSLDGNYWNYKNKDSVIGSPYEN
297 307 317 327 337
HAdV-D30K AVPFMPNSTAYPKIINNGTANPEDKKSAAKKTIVTNVYLGGDAGQPVATT
HAdV-D49K AVPFMPNSTAYPKIINNGTANPEDKKSAAKKTIVTNVYLGGDAAKPVATT
347 357 367 377
HAdV-D30K VSFNKETESNCVYSITFDFAWNKTYKNVPFDSSSLTFSYIAQDAEDKNE
HAdV-D49K ISFNKETESNCVYSITFDFAWNKTYKNVPFDSSSLTFSYIAQDAEDKNE
B
C
D
E238
Q331, G330
E
K238
K331, A330
F
CHO-CAR
Percentage of Cells Positive for GFP
100
80
60
40
20
0
HAdV-C5
HAdV-C5.KO1
HAdV-C5/D30K
HAdV-C5/D49K
HAdV-C5/D49.KO1.K
Uninfected
G
CHO-K1
100
80
60
40
20
0
HAdV-C5
HAdV-C5.KO1
HAdV-C5/D30K
HAdV-C5/D49K
HAdV-C5/D49.KO1.K
Uninfected

Figure 4

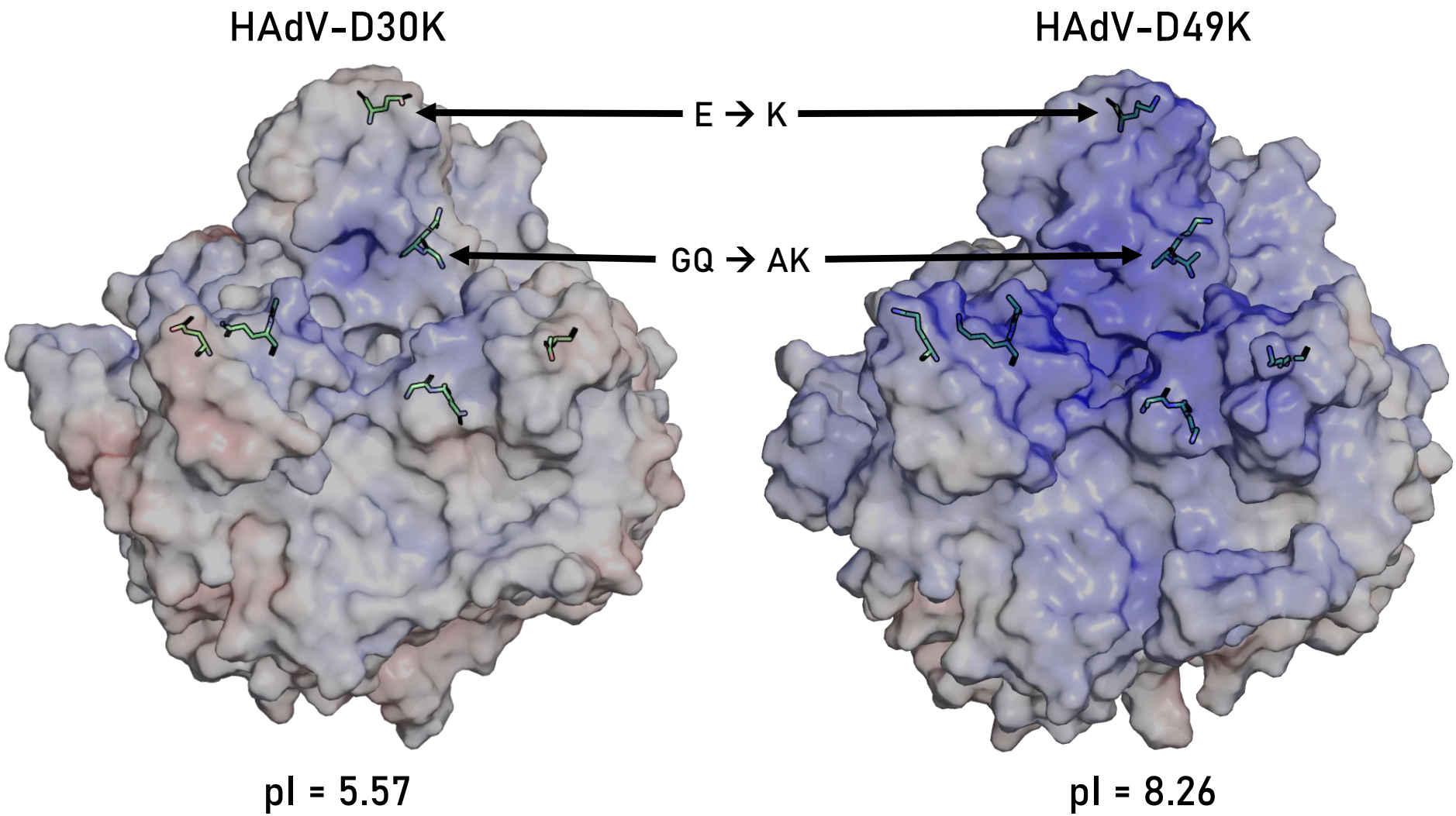


Figure 5

Table 1: Single crystal diffraction data collection statistics for fiber knob crystal structures determined in this study.

| PDB Entry | 6STU – HAdV-D30K | 6QPN – HAdV-D49K | 6QPO – HAdV-D49K.KO1 |
|---|---|---|---|
| **Data Collection** | | | |
| Diamond Beamline | I03 | I03 | I03 |
| Date | 18/04/2019 | 2017-02-27 | 2017-02-27 |
| Wavelength | 0.95372 | 0.97628 | 0.97628 |
| **Crystal Data** | | | |
| Crystallisation Conditions | 0.1M SPG, 25% w/v PEG 1500 | | |
| pH | 6.0 | 8.0 | |
| *a,b,c* (Å) | 63.35, 87.36, 217.86 | 106.83, 56.28, 115.70 | 105.17, 55.99, 116.03 |
| $\alpha=\beta=\gamma$ (°) | 90, 90, 90 | 90.00, 112.95, 90.00 | 90.0, 112.47, 90.0 |
| Space group | $P\ 2_1\ 2_1\ 2_1$ | P 1 2 1 | P 1 2 1 |
| Resolution (Å) | 2.39 – 54.76 | 2.74 – 106.54 | 2.45 – 57.07 |
| Outer shell | 2.39 – 2.45 | 2.74 – 2.81 | 2.45 - 2.51 |
| *R*-merge (%) | 0.116 (1.376) | 8.2 (163.3) | 9.7 (127.4) |
| *R*-meas (%) | 0.134 (1.583) | 9.7 (191.0) | 11.4 (149.9) |
| CC1/2 | 0.998 (0.623) | 0.981 (0.400) | 0.994 (0.491) |
| I / σ(I) | 11.2 (1.4) | 6.8 (1.0) | 9.2 (1.2) |
| Completeness (%) | 100.0 (100.0) | 99.1 (98.9) | 99.3 (99.3) |
| Multiplicity | 7.5 (7.8) | 3.7 (3.7) | 3.7 (3.7) |
| Total Measurements | 365,880 (28,110) | 122,219 (9,179) | 168,773 (12,231) |
| Unique Reflections | 48,897 (3,589) | 33,350 (2,461) | 45,958 (3,349) |
| Wilson B-factor($Å^2$) | 48.7 | 68.9 | 59.9 |
| **Refinement Statistics** | | | |
| Total number of refined | 9,637 | 9,346 | 9,363 |
| R-work reflections | 46,478 | 31,740 | 43,733 |
| R-free reflections | 2,348 | 1,609 | 2,225 |
| R-work/R-free (%) | 21.7 / 26.8 | 22.0 / 26.2 | 19.2 / 25.6 |
| **rms deviations** | | | |
| Bond lengths (Å) | 0.010 | 0.009 | 0.012 |
| Bond Angles (°) | 1.722 | 1.785 | 1.974 |
| [1]Coordinate error | 0.293 | 0.438 | 0.289 |
| Mean B value ($Å^2$) | 58.7 | 94.2 | 76.9 |
| **Ramachandran Statistics** | | | |
| Favoured/allowed/Outliers | 1122 / 78 / 8 | 1121 / 55 / 12 | 1097 / 82 / 9 |
| % | 92.88 / 6.46 / 0.66 | 94.4 / 4.6 / 1.0 | 92.3 / 6.9 / 0.8 |

Table 2: Comparison of transduction of various cancer cell lines by HAdV-C5 and HAdV-C5/D49K. *= P<0.05, **=P<0.01, ***=P<0.001, ****=P<0.0001, ns=not significant

| **Cancer Type** | **Cell Line Name** | **Level of HAdV-C5 Infection (RLU/mg total protein)** | **Level of HAdV-C5/D49K Infection (RLU/mg total protein)** | **Change in infectivity ( Fold change HAdV-C5/D49K divided by HAdV-C5 RLU/mg)** | **Statistical Significance (p value)** |
|---|---|---|---|---|---|
| Pancreatic Adenocarcinoma, derived from acitic metastasis | ASPC1 | 3.9E+04 | 1.2E+06 | 30.7 | ** |
| Pancreatic Adenocarcinoma | BXPC3 | 1.2E+04 | 2.5E+06 | 210.9 | ** |
| Pancreatic Adenocarcinoma | Panc10 | 1.0E+05 | 7.2E+06 | 69.2 | **** |
| Pancreatic Adenocarcinoma, derived from splenic metastasis | SW1990 | 9.6E+04 | 1.1E+06 | 11.3 | **** |
| Pancreatic Adenocarcinoma | MIA PaCa2 | 3.4E+05 | 1.4E+06 | 4.2 | ** |
| Pancreatic Adenocarcinoma, derived from liver metastasis | Suit2 | 6.0E+04 | 1.3E+06 | 22.2 | * |
| Pancreatic Ductal Adenocarcinoma | PANC 0403 | 1.2E+04 | 4.0E+05 | 33.0 | * |
| Pancreatic Ductal Adenocarcinoma, Derived from liver metastasis | CFPAC-1 | 1.8E+04 | 1.1E+06 | 62.0 | *** |
| Pancreatic Ductal Adenocarcinoma | PT45 | 3.9E+05 | 2.0E+06 | 5.1 | ** |
| Breast Carcinoma | BT-20 | 1.8E+03 | 8.6E+05 | 481.2 | * |

| | | | | | |
|---|---|---|---|---|---|
| Breast Ductal Carcinoma | BT-474 | 6.5E+03 | 1.4E+05 | 21.8 | * |
| Breast Adenocarcinoma, derived from brain metastasis | MDA-MB-361 | 2.2E+05 | 1.5E+06 | 6.7 | ** |
| Breast Adenocarcinoma, derived from plural effusion metastasis | MDA-MB-231 | 3.3E+04 | 1.5E+05 | 4.6 | * |
| Breast Adenocarcinoma, derived from plural effusion metastasis | MCF7 | 1.3E+04 | 6.6E+06 | 497.3 | *** |
| Large Lunge Cell Carcinoma | NCI-H460 | 2.1E+05 | 3.9E+06 | 18.8 | * |
| Lung Carcinoma | A427 | 1.2E+07 | 7.2E+06 | 0.6 | * |
| Lung Carcinoma | A549 | 2.8E+06 | 6.9E+06 | 2.5 | *** |
| Esophageal Squamous Cell Carcinoma | Kyse-30 | 6.3E+05 | 1.4E+07 | 22.4 | *** |
| Colorectal Adenocarcinoma, Duke's Type C | DLD-1 | 6.0E+06 | 5.0E+06 | 0.8 | **ns** |
| Ovarian Adenocarcinoma | SKOV-3 | 9.1E+05 | 7.7E+06 | 8.5 | ** |